NJC

PAPER

View Article Online
View Journal | View Issue

Cite this: *New J. Chem.*, 2017, 41, 1558

Theranostic hexosomes for cancer treatments: an *in vitro* study

Valeri Meli,*[a] Claudia Caltagirone,[a] Chiara Sinico,[b] Francesco Lai,[b] Angela M. Falchi,[c] Maura Monduzzi,[a] Marc Obiols-Rabasa,[d] Giacomo Picci,[a] Antonella Rosa,[c] Judith Schmidt,[e] Yeshayahu Talmon[e] and Sergio Murgia*[a]

Received 14th October 2016,
Accepted 28th December 2016

DOI: 10.1039/c6nj03232j

www.rsc.org/njc

We have formulated and investigated innovative lipid-based nanoparticles characterized by a reverse hexagonal liquid crystalline inner structure (hexosomes). These nanoparticles were doped with a potent, highly water insoluble anticancer drug, namely docetaxel, and stabilized by a mixture of commercial and folate- and rhodamine-conjugated Pluronic F108. Thus, they simultaneously possess therapeutic, imaging, and targeting properties toward cancer cells. The morphological and structural aspects of the hexosomes were investigated at different temperatures (10, 25, 37, and 50 °C), and our results demonstrate good performance in terms of stability of these nanoparticles. The latter was furthermore confirmed by the very slow and continuous release profile of docetaxel observed in drug release experiments. Although it was not possible to assess a specific compartmentalization of the dye, this formulation allowed the successful visualization of HeLa cells. Finally, cytotoxic assays showed a 20-fold higher toxic effect of the drug-doped hexosomes against HeLa cells with respect to the free (not loaded in hexosomes) anticancer drug. On the whole, these results indicate that this formulation is a potential theranostic tool in oncology.

1. Introduction

The field of dispersed lipid liquid crystalline phases for biomedical applications is dominated by lamellar phase dispersions, namely liposomes. Indeed, they have been widely studied as model membranes,[1,2] templates,[3] and transporters for drugs.[4] From a clinical perspective, this huge effort of research has translated into several marketed liposomal formulations, mainly for anticancer applications (Doxil, Caelyx, and Myocet are liposome-based formulations widely used in the treatment of different types of cancer including Kaposi's sarcoma, ovarian cancer, and myeloma).[5] Remaining in the lipid liquid crystalline phases arena, aqueous dispersions of reverse bicontinuous cubic phases, commonly known as cubosomes, were, in the past, deeply investigated from a physicochemical point of view,[6–9] and more recently proposed for biomedical uses.[10–12] Hexosomes, dispersions of the reverse hexagonal phase, represent another example of liquid crystalline nanoparticles. They are composed of water cylinders enveloped by lipid monolayers and arranged in a two-dimensional hexagonal architecture. Similarly to cubosomes, hexosomes can be formulated by dispersion in a multiphase region, where the liquid crystalline phase coexists with water. Although a variety of lipids can form reverse hexagonal phases, they (also in excess of water) are often thermodynamically stable only at high temperature, as found in the monoolein (MO)/water or phytantriol (PHYT)/water binary phase diagrams.[13,14] The formation of this phase at room temperature generally requires the addition of a lipophilic molecule to the dispersion (*e.g.*, oleic acid, OA) that may alter the MO or PHYT effective packing parameter, thus inducing the reverse bicontinuous cubic to reverse hexagonal phase transition.[15–23] In addition, several examples in the literature describe how appropriate modification of the PHYT chain can lead to the formation of a hexagonal structure.[24–26]

The colloidal stability of hexosomes (and cubosomes as well) is achieved by the action of stabilizing polymers. These polymers may have a role in reducing the rate of clearance of the nanostructures from the bloodstream by plasma proteins, but their primary function is to promote steric stabilization against aggregation. The most diffuse polymers used for such a purpose are

[a] *Department of Chemical and Geological Science, University of Cagliari, CNBS and CSGI, s.s. 554 bivio Sestu, 09042, Monserrato (CA), Italy. E-mail: murgias@unica.it*
[b] *Department of Life and Environmental Sciences, University of Cagliari, via Ospedale 72, 09124 Cagliari, Italy*
[c] *Department of Biomedical Science, University of Cagliari, s.s. 554 bivio Sestu, 09042 Monserrato (CA), Italy*
[d] *Division of Physical Chemistry, Department of Chemistry, Center for Chemistry and Chemical Engineering, Lund University, P.O. Box 124, SE-221 00 Lund, Sweden*
[e] *Department of Chemical Engineering, Technion – Israel Institute of Technology, Haifa 32000, Israel*

Pluronics, especially F127 and F108, which differ in their HLB (hydrophilic–lipophilic balance) value, which is lower for F127.[27,28] Other stabilizing agents are also employed, such as DSPE-PEG_{2000}[29] and Citrem.[30]

Hexosomes of various compositions were studied as drug nanocarriers. For instance, the release of irinotecan (a water-soluble anticancer drug) from oleyl glycerate-based hexosomes was reported,[31] and MO/OA-based hexosomes were proposed for oromucosal delivery of progesterone and for improving the skin penetration of a model protein (cyclosporin A).[32,33] Hexosomes containing the BDNF protein were also formulated.[34] More recently, hexosomes based on diethylenetriamine pentaacetic acid and PHYT, able to complex Gd(III) and targeted with an α-Flag antibody fragment for antigen recognition, were developed as MRI imaging tools.[25] To the same aim, nitroxide-loaded MO-based hexosomes were designed. *In vivo* MRI imaging tests were conducted on mice using these nanoparticles to investigate the biodistribution after intravenous administration.[35,36] Cancer cell-targeted hexosomes were also engineered as a potential theranostic platform by simultaneously combining the therapeutic action of camptothecin and the fluorescence imaging functionality of a pyrene-modified BODIPY.[37]

Docetaxel (DTX) is an important chemotherapeutic agent against many locally advanced and metastatic cancers. However, its clinical applications are drastically limited by its extremely low water solubility[38] and non-selective mode of action, which leads to several side effects due to acute toxicity to healthy cells. During the last decade, several drug delivery systems have been developed to enhance DTX water solubility and reduce toxicity, including polymeric and lipid nanocarriers.[39]

In this context, we present here a MO-based hexosomes formulation loaded with DTX, and stabilized in aqueous medium by a mixture of commercial rhodamine-conjugated and folate-conjugated Pluronic F108. This innovative system was developed with the aim to enhance the aqueous solubility and bioavailability of DTX by means of its encapsulation in the stable liquid crystalline structure of hexosomes with long-term circulation properties. Indeed, the prepared hexosomes were adequately large in size to elude fast renal clearance while their nanoparticulate structure was enveloped within a highly flexible and hydrophilic polymeric layer of Pluronic F108, which should confer them stealth properties, thus avoiding opsonisation and consequent clearance from the systemic circulation. Further, to make them suitable as both therapeutic and diagnostic tools in cancer treatment, hexosome particles were functionalized with targeting and imaging moieties, namely folic acid and rhodamine. Folate was selected as a tumour-targeting ligand since it is a small, non-toxic, non-immunogenic molecule, whose receptors are often over-expressed in cancer cells.[40]

DTX-loaded hexosomes were characterized for size, morphology, and structural features by SAXS and cryo-TEM.[41–44] The drug stability in the liquid crystalline matrix was evaluated by *in vitro* release studies. Finally, HeLa cells were employed to evaluate cytotoxicity and cellular uptake.

2. Materials and methods

2.1 Materials

Monoolein (MO, 1-monooleoylglycerol, RYLO MG 19 PHARMA, glycerol monooleate, 98.1 wt%) was kindly supplied by Danisco A/S, DK-7200, Grinsted, Denmark. Pluronic F108 (PF108, PEO132-PPO50-PEO132), docetaxel (≥97%), oleic acid (OA, 99%), acetonitrile (≥99.9%), ethanol (≥99.8%), and acetic acid (≥99.7%) were purchased from Sigma-Aldrich. Distilled water purified by means of a Milli-Q system (Millipore) was used for sample preparation. The syntheses of PF108-FA and PF108-R have been reported elsewhere.[45,46]

2.2 Hexosome preparation and characterization

MO-based hexosomes were formulated and stabilized by dispersing the appropriate amount of MO and OA in water solution of a mixture of Pluronic F108, folate-conjugated and rhodamine-conjugated F108 (PF108/PF108-FA/PF108-R) under 10 min ultrasonic radiation treatment using a processor UP100H by Dr Hielscher, mode of cycle 0.9, amplitude 90%. The PF108/PF108-FA/PF108-R ratio was 80/20/0 and 60/20/20, respectively, for non-fluorescently marked hexosomes (HEX) and rhodamine marked hexosomes (HEX-R). Docetaxel doped hexosomes (HEX-R/DTX) were produced by dispersing the active molecule in the melted lipid phase kept in an ultrasonic bath and then mixed with the Pluronic solution. The final volume (4 mL) composition was approximately 96.4 wt% water, 2.97 wt% MO, 0.33 wt% OA and 0.3 wt% Pluronic mixture.

Dynamic light scattering (DLS) measurements for the determination of the nanoparticle size and polydispersity index were performed at 10, 25, 37, and 50 °C using a light scattering goniometer instrument (3D LS Instruments, Fribourg, Switzerland), which was equipped with a 35 mW He–Ne laser light source (wavelength of 632.8 nm). The characterization of the internal structure of the nanoparticles at 10, 25, 37, and 50 °C was carried out by small angle X-ray scattering (SAXS) using a Ganesha 300XL (SAXSLAB ApS, Skovlunde, Denmark). The scattering data were collected over the q range of $0.014 < q\ (\text{Å}^{-1}) < 0.753$, where the magnitude of the scattering vector, q, is defined as $q = (4\pi/\lambda)\sin(\theta/2)$, where θ is the scattering angle. Silver behenate (CH_3–$(CH_2)_{20}$–COOAg) with a d spacing value of 58.38 Å was used as a standard to calibrate the angular scale of the measured intensity. The water channel radii of the reverse hexagonal phase were calculated using the relation $r_w = a(1 - \phi_{lip})^{1/2}(\sqrt{3}/2\pi)^{1/2}$, where a is the lattice parameter obtained from the SAXS analysis and ϕ_{lip} is the volume fraction of the dispersed phase. Samples were equilibrated for 1 h at the measurement temperature prior to performing the 2 h experiment. The morphology of the nanoparticles was observed by cryo-TEM at a120 kV acceleration voltage using an FEI Tecnai T12 G^2 transmission electron microscope at about −175 °C in the low-dose imaging mode to minimize electron-beam radiation-damage. Images were digitally recorded using a Gatan US1000 high-resolution CCD camera.[47]

2.3 Photophysical measurements

The photophysical measurements were performed after dilution of hexosome dispersions with Milli-Q water (1 : 100) by means of

a PerkinElmer LS 55 spectrofluorimeter to record the emission and excitation spectra. Rhodamine 6G dissolved in EtOH was used as a reference standard (Φ_{ref} = 0.95) to measure the fluorescence quantum yield on PF108-R. The absorption spectra were recorded on a Thermo Nicolet Evolution 300 spectrophotometer.

2.4 Drug release experiments

DTX release from the formulated hexosomes was investigated using a vertical Franz diffusion cell apparatus (LGA, Berkeley, CA) with a diffusion surface area of 0.75 cm^2 and a regenerated cellulose membrane, which was hydrated for 1 hour at room temperature before the experiments. The receptor compartment was filled with 5.5 mL of a water/ethanol mixture (50/20 v/v) and kept under stirring at 37 °C for increasing DTX solubility in the receiving phase thus ensuring pseudo-sink conditions throughout the release experiments. A 200 μL sample of hexosome dispersion was applied on the membrane and the experiment was run for 8 hours under non-occlusion conditions. At time intervals of 1 hour, the receiving phase was withdrawn and replaced by an equal volume of the water/ethanol mixture pre-equilibrated at 37 °C to maintain sink conditions. The withdrawn solutions were analysed by HPLC to quantify the DTX content, as described below. At the end of the experiments, the hexosome formulations were removed from the membrane surface and analysed to check the particle average diameter and size distribution. Experiments were performed in triplicate.

2.5 Determination of MO, OA and DTX contents in hexosomes

DTX-loaded hexosomes were separated from the non-incorporated drug by dialysis against water using cellulose tubing. Dialysis bags with a 14 KDa molecular weight cut off were loaded with 2 mL of hexosome dispersion and kept in water at room temperature (25 °C) for 2 hours. The water (1 L) was changed after 1 h to allow the dissolution and consequent removal of free DTX. For analysis, 10 μL aliquots of the dialyzed dispersions were dissolved in 300 μL of CH_3CN with 0.14% CH_3COOH (v/v), vortexed to obtain a clear solution, and then injected (20 μL) into a Agilent Technologies 1100 high performance liquid chromatograph equipped with a diode array detector (Agilent Technologies, Palo Alto, CA), set up using a previously described method. Briefly, MO, OA, and DTX in hexosome dispersions were quantified using a XDB-C_{18} Eclipse (150 × 4.6 mm, 3.5 mm particle size) (Agilent Technologies) column equipped with a Zorbax XDB-C_{18} Eclipse (12.5 × 4.6 mm, 5 mm particle size) guard column (Agilent Technologies), thermostated at 37 °C. The mobile phase was a $CH_3CN/H_2O/CH_3COOH$ (75/25/0.12, v/v/v) mixture, pumped at 2.3 mL min^{-1}. The absorbance was recorded at 200 nm for MO and OA detection and at 230 nm for DTX detection. Chromatograms were recorded and integrated by using the Agilent OpenLAB Chromatography acquisition data system.

Drug encapsulation efficacy (EE%) was calculated by using the following equation: EE% = (weight of the drug-loaded hexosomes)/(weight of the feeding drug) × 100%. Data were expressed as a mean ± standard deviation (SD) of three independent experiments involving duplicate analyses for each sample.

2.6 Cell culture

HeLa cells (ATCC collection) were cultured at 37 °C under a humidified 5% CO_2 atmosphere in high-glucose phenol red-free Dulbecco's modified Eagle's medium (DMEM, Molecular Probes, USA) containing 10% (v/v) foetal bovine serum, 100 U mL^{-1} penicillin and 100 μg mL^{-1} streptomycin (Invitrogen). Live cell imaging was performed with HeLa cells seeded in 35 mm plates two days before the experiments, when the cell density had reached 90% confluency. After addition of DTX loaded-hexosomes at a concentration of 1 : 500 (2 μL in 1 mL of fresh medium), the cells were incubated at 37 °C for 4 h. Before the imaging session, the extracellular hexosome suspension was replaced with fresh serum-free medium.

2.7 Fluorescence microscopy

Light microscopy visualizations were carried out using a Zeiss (Axioskop) upright fluorescence microscope (Zeiss, Oberkochen, Germany) equipped with 10×, 20× and 40×/0.75 NA water immersion objectives and a HBO 50 W L-2 mercury lamp (Osram, Berlin, Germany). Twelve-bit-deep images were acquired using a monochrome cooled CCD camera (QICAM, Qimaging, Canada). Filters used for dye fluorescence observations were: ex 546 ± 6 and em 620 ± 60. Digital images were processed using Image Pro Plus software (Media Cybernetics, Silver Springs, MD).

2.8 Cytotoxic activity (MTT assay)

The *in vitro* cytotoxicity of hexosome formulations was evaluated by the MTT (3-(4,5-dimethylthiazol-2-yl)-2,5-diphenyltetrazolium bromide) reduction assay using HeLa cells. Cells were seeded onto 24-well plates with a 3×10^4 cells per well density in 500 μL of serum-containing media. Two days after seeding, when a cell confluence of 90% was attained, experiments were carried out by adding the different formulations to the cells at a concentration of 1 : 500 (2 μL in 1 mL of serum-free medium) and then incubating at 37 °C for 4 h. The effect of docetaxel 10 μM (precisely, 1 μL of a 10 mM DTX solution in DMSO was added to 1 mL of serum-free medium) on HeLa cell viability was also measured at the same incubation time, as the control. A 50 μL MTT water solution (5 mg mL^{-1}) was then added and left for 2 h at 37 °C. Finally, the medium was aspirated, the formed coloured formazan crystals were dissolved with 500 μL of DMSO and their concentration was spectrophotometrically quantified at 570 nm using an Infinite 200 auto microplate reader (Infinite 200, Tecan, Austria). The absorbance is proportional to the number of viable cells. The results are shown as the percentage of cell viability in comparison with non-treated control cells. Data were expressed as mean ± standard deviation (SD) of three independent experiments involving quadruplicate analyses for each sample.

2.9 Statistical analysis

The evaluation of statistical significance of differences was performed using Graph Pad INSTAT software (GraphPad software, San Diego, CA, USA). Comparison between groups was assessed by one-way analysis of variance (one-way ANOVA) followed by the Bonferroni multiple comparisons test.

3. Results and discussion

3.1 Hexosome physicochemical and photophysical characterization

In this work, an innovative hexosome formulation was characterized from a structural and technological point of view. The formulation was obtained by firstly mixing in melted monoolein (MO) oleic acid and the anticancer drug docetaxel (DTX), and then dispersing with a tip sonicator the obtained lipid phase in an aqueous solution of Pluronic F108, folate-conjugated and rhodamine-conjugated F108 (PF108/PF108-FA/PF108-R) in a ratio of 60/20/20 (80/20/0 for non-fluorescently marked hexosomes). Fig. 1 shows a cryo-TEM image representative for such a hexosome formulation. The examination of this image reveals several spherical and quasi-spherical nanoparticles showing an inner structure denoted by the hexagonal motifs and curved striations that are commonly observed in liquid crystalline nanoparticles characterized by the reverse hexagonal symmetry. Though conclusive evidence is still missing, such striations are supposed to be derived from the deformation of the hexagonally packed water cylinders. This configuration may be adopted to better stabilize the hexosomes, allowing a uniform hydrophobic surface of the nanoparticles that can be easily stabilized by PF108 adsorption. This avoids the less favourable condition of stabilizing the terminal ends of the cylinders, where both hydrophilic and hydrophobic moieties of MO are exposed to water. However, nanoparticles showing hexagonally packed water cylinders at the surface are sometimes observed, demonstrating that the latter configuration is also possible.[7,48]

The size and structural features of the hexosomes were studied by DLS and SAXS. Moreover, since this formulation is proposed for theranostic nanomedicine, investigating its stability at different temperatures seemed to be important. The results are reported in Table 1 and Fig. 2.

The SAXS experiments proved the hexagonal inner structure of the formulation. Indeed, the diffraction pattern at 25 °C (Fig. 2) is characterized by three Bragg peaks at a q ratio of $1:\sqrt{3}:2$, consistent with the reverse hexagonal phase.

Table 1 reports the lattice parameter, a, obtained from the SAXS experiments as well as the calculated radius of the water channels, r_w, (see the Materials and methods section). These experiments were performed with the following temperature cycle: 25, 37, 50, 10, 25, and 37 °C.

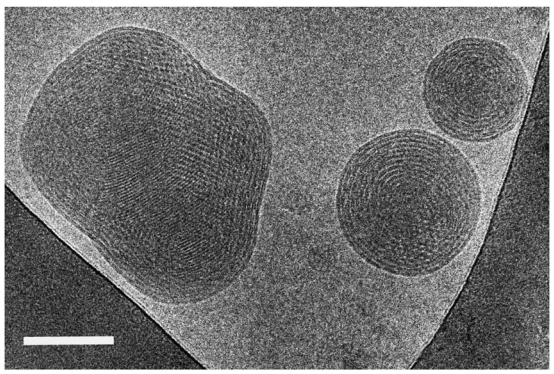

Fig. 1 Cryo-TEM image of the hexosome formulation stabilized (at 25 °C) using a 60/20/20 mixture of commercial PF108, folate-conjugated, and rhodamine-conjugated PF108, and loaded with docetaxel. The bar is 100 nm.

Table 1 Hexosome lattice parameters (a), radius of the water channels (r_w), average hydrodynamic radius (R_h), and polydispersity index (PdI) at different temperatures

T (°C)	a (Å)	r_w (Å)	R_h (nm)	PdI
25	60.0 ± 0.1	31.0 ± 0.1	109	0.12
37	58.1 ± 0.1	30.0 ± 0.1	106	0.16
50	56.3 ± 0.1	29.0 ± 0.1	104	0.12
10	—	—	105	0.27
25	60.4 ± 0.2	31.1 ± 0.1	—	—
37	59.1 ± 0.1	30.5 ± 0.1	—	—

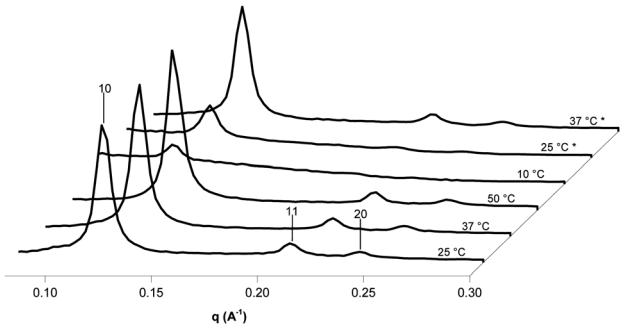

Fig. 2 SAXS diffraction patterns of the same hexosome formulation described in Fig. 1 recorded according to the following temperature cycle: 25, 37, 50, 10, 25, and 37 °C (see the text). The Miller indices are reported on top of the corresponding Bragg peaks.

Basically, the reverse hexagonal nanostructure was observed at all the investigated temperatures, though a slight decrease of the lattice parameter was detected as the temperature is increased. Such a behaviour, already reported in the literature, is related to the greater disorder of the monoolein alkyl chains at higher temperatures, which leads to a higher negative curvature of the lipid/water interface.[49] However, it should be noticed that the intensity of the diffraction pattern collected at 10 °C is greatly reduced compared to that obtained at higher temperatures, so the reflections corresponding to the 11 and 20 planes almost vanished. This fact suggests some kind of alteration of the sample in terms of aggregation of the nanoparticles, or the loss of the symmetry of their inner phase.

The DLS results reported in Table 1 demonstrate that the formulation is essentially not sensitive to the temperature variations, since the average size and polydispersity index (PdI) of the nanoparticles did not change upon increasing the temperature from 25 to 37 to 50 °C. At the same time, the huge increase in the PdI recorded at 10 °C supports the idea that aggregation of the nanoparticles occurred at this temperature. Remarkably, the nanostructural features as determined by SAXS are recovered after returning to room temperature.

Rhodamines belong to the family of the xanthene dyes. Due to strong absorption in the visible region, high fluorescence quantum yield (Φ = 0.95 in EtOH for rhodamine 6G)[50] as well as good optical and thermal stability, they have been extensively

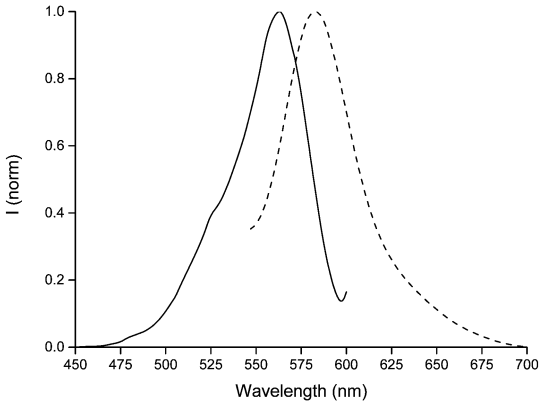

Fig. 3 Normalized excitation (solid line, λ_{em} = 620 nm) and emission (dashed line, λ_{exc} = 522 nm) spectra of the aqueous hexosome formulation stabilized using a PF108/PF108-FA/PF108-R ratio = 60/20/20 (wt%).

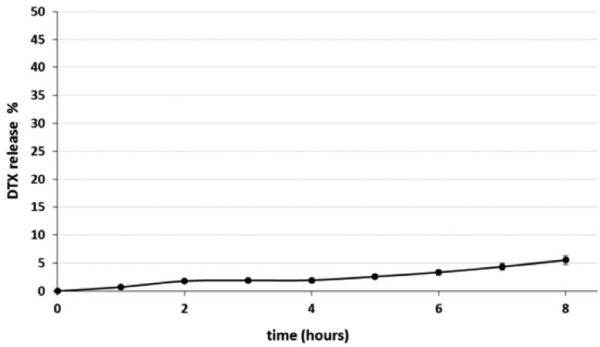

Fig. 4 Release profile of docetaxel (DTX) from hexosomes at 37 °C as a function of time.

employed as lasing media in liquid and solid-state dye lasers.[51] However, the self-assembly aggregation process between individual dye molecules often minimizes the performance efficiency.[52] Although for some applications rhodamines are used in the free form, often the probes must be modified *via* a synthetic path, and the absorption and emission properties can be strongly influenced by substituents in the xanthene skeleton.[53]

The photophysical properties of PF108-R were investigated in our previous work.[46] In chloroform and water, PF108-R shows the same strong absorption at 560 nm, with a shoulder at 522 nm. The emission band generated at 584 nm in chloroform, upon excitation at 522 nm, underwent a red-shift in water at 594 nm, as a result of the increased polarity of the medium. The measured quantum yields (0.16 and 0.58, in water and chloroform, respectively) show that Pluronic conjugation has a negative effect on the emission efficiency of the dye (for its precursor rhodamine B, Φ = 0.31 in water[54] and Φ = 0.65 in basic EtOH).[50]

The hexosome formulation was characterized from the photophysical point of view after 1 : 100 dilution in water to minimize the light scattering due to the bluish nature of the sample (Fig. 3). Upon excitation at 522 nm a band centred at 583 nm arises. Considering the strong similarities in the photophysical properties of PF108-R in chloroform and the fluorescent hexosomes in water, in the latter case it can be envisaged that the PF108-conjugated fluorophore is embedded in the poly(ethylene oxide) corona surrounding the nanoparticles, thus experiencing quite an apolar environment. By setting the emission wavelength to 620 nm, the recorded excitation spectrum overlapped the absorption spectra of PF108-R in chloroform and in water.

3.2 *In vitro* release study

The *in vitro* release study was carried out to assess both the stability of the drug in the hexosome nanostructures and the ability of the carrier to modulate the release rate of the incorporated drug. DTX release is expected to take place only from the lipid phase because of the poor water solubility of this drug. To evaluate the *in vitro* DTX release from the hexosome formulation, a large amount of formulation (200 μL) was applied on the membrane surface following the infinite dose technique, which prevents drug reduction in the donor compartment during the experiment, thus securing a constant driving force for the diffusion process through the matrix and gives steady-state conditions. The drug percentage released from the hexosomes as a function of time during 8 h, is reported in Fig. 4. As can be seen from the graph, the drug release exhibited a linear profile characterized by a very slow and continuous release rate. Such a behaviour is remarkable, since it differentiates this formulation from others of the same kind, commonly characterized by an initial burst release.[55]

After the 8 h experiment only 6% of the applied dose was recovered from the receptor compartment, thus demonstrating stable entrapment of the drug into the hexosome formulation. DTX recovery from the donor and receptor compartment was always more than 95–97% of the applied dose, and DLS analyses did not show any significant alteration in the hexosome size and polydispersity after an 8 h experiment. This studied period gives significant information to predict the stability during the distribution process, since the *in vivo* study with monoolein-based liquid crystalline nanoparticles demonstrated a high accumulation of carrier systems to tumour mass after less than 8 h.[55]

3.3 HeLa cell imaging and cytotoxic activity

The investigation of the hexosome internalization within HeLa cells was conducted by fluorescence microscopy. As can be noticed in Fig. 5, while no fluorescence was detected in untreated-control cells, a faint diffuse fluorescence was observed within the cellular cytoplasm after 4 h incubation with the fluorescent hexosomes (not loaded with the drug). Differently from other fluorescent microscopy experiments performed on HeLa cells using similar liquid crystalline formulations loaded with hydrophobic dyes embedded in the lipid portion of the nanoparticles,[37,56] here it was not possible to assess a specific compartmentalization of the dye within the cells after endosomal/lysosomal degradation of the hexosomes. This fact may be related to the nature of the dye (conjugated to the Pluronic) used in this work. Indeed, while hydrophobic dyes invariably localize in the lipid droplets (dynamic storage organelles representing the intracellular reservoir of apolar lipids), here the surfactant nature of the rhodamine-conjugated F108 probably allowed its partition in the cytoplasmic membranes, thus leading to the observed lack of a definite localization.

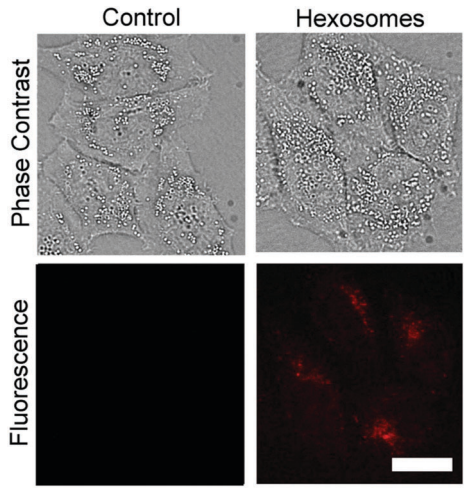

Fig. 5 Fluorescence microscopy of living HeLa cells treated with hexosomes not carrying the drug (incubation for 4 h) showing a diffuse cytoplasmic fluorescence in treated cells indicating nanoparticle uptake. Scale bar = 20 μm.

The amount of MO, OA (expressed as mg mL^{-1} of dispersion), and DTX (μg mL^{-1}) in different hexosome formulations was checked by HPLC-DAD. The analysis was performed on the hexosome formulations stabilized either with the mixture PF108/PF108-FA (HEX) or with the mixture PF108/PF108-FA/PF108-R (HEX-R), and also on the latter formulation loaded with DTX (HEX-R/DTX).

The monoolein concentration in HEX, HEX-R, and HEX-R/DTX formulations was found to be 31.4 ± 2.9 mg mL^{-1}, while OA concentration measured in the same series of nanoparticle formulations was 3.8 ± 0.3 mg mL^{-1}.

Drug concentration in the HEX-R/DTX formulation was found to be 203.7 ± 27.28 μg mL^{-1}, while the DTX/MO molecular ratio was 1/6.5 and the encapsulation efficacy (EE%) was 68 ± 9%.

The cytotoxicity of these formulations was tested in HeLa cells, by means of the MTT assay. Fig. 6 shows the viability, expressed as % of the control, of HeLa cancer cells after 4 h of incubation with the nanoparticle formulations at a concentration of 2 μL mL^{-1} of medium (corresponding to 63 μg mL^{-1} of MO). The cytotoxic effect of DTX 10 μM was also measured at 4 h-incubation for comparison. The results of these experiments showed that the treatment with the HEX-R formulations did not significantly reduce cell viability, in comparison with the control (Ctrl, not treated with nanoparticles). On the contrary, the incubation with HEX-R/DTX particles caused a statistically significant reduction in HeLa cell viability (24% of reduction) with respect to the control. This fact is due to the presence of the anticancer drug. Indeed, a significant cytotoxic effect (28% reduction in cell viability) was also observed in cells treated with a 10 μM solution of the free antitumor drug. Remarkably, when the HeLa cells were treated with DTX-loaded hexosomes (DTX dose of approximately 0.5 μM) a cytotoxic effect comparable to that of the free drug tested at a much higher (20-fold) concentration was observed. These results are in good agreement with those reported by Muir *et al.*[36]

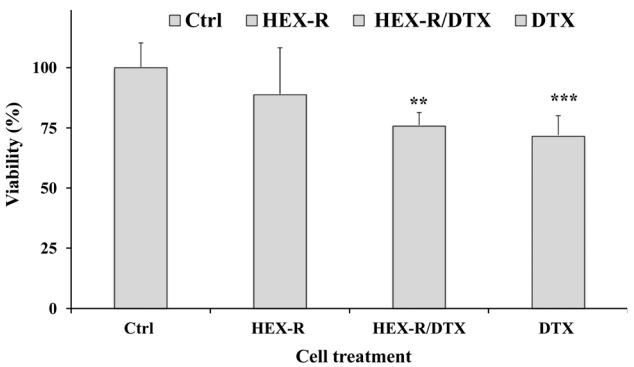

Fig. 6 Viability, expressed as % of the control, induced in HeLa cells by incubation for 4 h in the presence of different types of hexosome formulations (HEX-R, and HEX-R/DTX, see the text) and docetaxel (DTX). The drug concentration in the HEX-R/DTX formulation (0.5 μM) is 20-fold lower than that in DTX solution (10 μM). The results are expressed as mean ± standard deviation (SD) of four independent experiments involving quadruplicate analyses for each sample (n = 4). *** = $P < 0.001$; ** = $P < 0.01$ *versus* Ctrl, and data were analysed using one-way ANOVA.

4. Conclusions

Monoolein is a polar lipid widely used in formulating a variety of systems with potential pharmaceutical applications.[56–59] Among these, cubosomes and hexosomes possibly represent the most outstanding systems because of numerous features that can be profitably exploited in theranostic nanomedicine. These include a viscosity of the dispersion similar to water (an essential characteristic for i.v. administration) as well as the possibility of simultaneously loading the nanoparticles with drugs and imaging probes while decorating their surface with targeting moieties. Despite the almost identical composition of cubosomes and hexosomes, an increasing amount of evidence demonstrates different biological impacts that these only apparently similar nanoparticles have in terms of cytotoxicity[60–62] and biodistribution.[63] These emerging peculiarities could be of the highest importance with respect to possible pharmaceutical applications, and could be used, for example, to address hexosomes and cubosomes towards different biological targets.

In this paper, we proved that monoolein-based hexosomes can be loaded with docetaxel, a highly hydrophobic anticancer drug, and stabilized by a mixture of commercial and derivatized Pluronics conjugated to fluorescent (rhodamine) and cancer cell targeting (folate residues) moieties while keeping the specific liquid crystalline features of their inner nanostructure unaltered. The high stability of this formulation was also demonstrated by release experiments, showing a very slow and continuous profile without an initial burst release of the drug. In addition, cytotoxicity tests proved the efficacy of this formulation against HeLa cells, being 20-fold more active than the docetaxel administered in solution. These results confirm that hexosomes are a most promising and useful platform for theranostic nanomedicine.

Acknowledgements

Financial support by Regione Autonoma della Sardegna (CRP-59699) is gratefully acknowledged. Sardegna Ricerche Scientific Park (Pula, CA, Italy) is acknowledged for free access to facilities of the Nanobiotechnology Laboratory. The cryo-TEM work was performed at the Technion Laboratory for Electron Microscopy of Soft matter, supported by the Technion Russell Berrie Nanotechnology Institute (RBNI). The authors acknowledge financial support from the European Commission under the Seventh Framework Program by means of the grant agreement for the Integrated Infrastructure Initiative No. 262348 European Soft Matter Infrastructure (ESMI).

Notes and references

1 M. Edidin, *Annu. Rev. Biophys. Biomol. Struct.*, 2003, **32**, 257–283.
2 F. Cuomo, A. Ceglie and F. Lopez, *J. Colloid Interface Sci.*, 2012, **365**, 184–190.
3 F. Cuomo, F. Lopez and A. Ceglie, *Adv. Colloid Interface Sci.*, 2014, **205**, 124–133.
4 K. Cho, X. Wang, S. Nie, Z. Chen and D. M. Shin, *Clin. Cancer Res.*, 2008, **14**, 1310–1316.
5 W. T. Al-Jamal and K. Kostarelos, *Acc. Chem. Res.*, 2011, **44**, 1094–1104.
6 J. Gustafsson, H. Ljusberg-wahren and M. Almgren, *Langmuir*, 1996, **12**, 4611–4613.
7 J. Gustafsson, H. Ljusberg-Wahren, M. Almgren and K. Larsson, *Langmuir*, 1997, **13**, 6964–6971.
8 C. Neto, G. Aloisi, P. Baglioni and K. Larsson, *J. Phys. Chem. B*, 1999, **103**, 3896–3899.
9 M. Monduzzi, H. Ljusberg-Wahren and K. Larsson, *Langmuir*, 2000, **16**, 7355–7358.
10 X. Mulet, B. J. Boyd and C. J. Drummond, *J. Colloid Interface Sci.*, 2013, **393**, 1–20.
11 I. D. Azmi, S. M. Moghimi and A. Yaghmur, *Ther. Delivery*, 2015, **6**, 1347–1364.
12 V. Miceli, V. Meli, M. Blanchard-Desce, T. Bsaibess, M. Pampalone, P. G. Conaldi, C. Caltagirone, M. Obiols-Rabasa, J. Schmidt, Y. Talmon, A. Casu and S. Murgia, *RSC Adv.*, 2016, **6**, 62119–62127.
13 H. Qiu and M. Caffrey, *Biomaterials*, 2000, **21**, 223–234.
14 J. Barauskas and T. Landh, *Langmuir*, 2003, **19**, 9562–9565.
15 M. Nakano, T. Teshigawara, A. Sugita, W. Leesajakul, A. Taniguchi, T. Kamo, H. Matsuoka and T. Handa, *Langmuir*, 2002, **18**, 9283–9288.
16 S. Mele, S. Murgia and M. Monduzzi, *Colloids Surf., A*, 2003, **228**, 57–63.
17 R. Angius, S. Murgia, D. Berti, P. Baglioni and M. Monduzzi, *J. Phys.: Condens. Matter*, 2006, **18**, S2203–S2220.
18 I. Amar-Yuli, E. Wachtel, E. Ben Shoshan, D. Danino, A. Aserin and N. Garti, *Langmuir*, 2007, **23**, 3637–3645.
19 Y. D. Dong, I. Larson, T. Hanley and B. J. Boyd, *Langmuir*, 2006, **22**, 9512–9518.
20 P. P. Wibroe, I. D. Mat Azmi, C. Nilsson, A. Yaghmur and S. M. Moghimi, *Nanomedicine*, 2015, **11**, 1909–1914.
21 C. Nilsson, J. Østergaard, S. W. Larsen, C. Larsen, A. Urtti and A. Yaghmur, *Langmuir*, 2014, **30**, 6398–6407.
22 S. Murgia, F. Caboi and M. Monduzzi, *Chem. Phys. Lipids*, 2001, **110**, 11–17.
23 B. Angelov, A. Angelova, R. Mutafchieva, S. Lesieur, U. Vainio, V. M. Garamus, G. V Jensen and J. S. Pedersen, *Phys. Chem. Chem. Phys.*, 2011, **13**, 3073–3081.
24 C. Fong, A. Weerawardena, S. M. Sagnella, X. Mulet, L. Waddington, I. Krodkiewska and C. J. Drummond, *Soft Matter*, 2010, **6**, 4727–4741.
25 M. J. Moghaddam, L. de Campo, M. Hirabayashi, P. A. Bean, L. J. Waddington, J. A. Scoble, G. Coia and C. J. Drummond, *Biomater. Sci.*, 2014, **2**, 924–935.
26 M. J. Moghaddam, L. de Campo, L. J. Waddington and C. J. Drummond, *Soft Matter*, 2010, **6**, 5915.
27 J. Y. T. Chong, X. Mulet, L. J. Waddington, B. J. Boyd and C. J. Drummond, *Soft Matter*, 2011, **7**, 4768.
28 T. Landh, *J. Phys. Chem.*, 1994, **98**, 8453–8467.
29 N. Zeng, Q. Hu, Z. Liu, X. Gao, R. Hu, Q. Song, G. Gu, H. Xia, L. Yao, Z. Pang, X. Jiang, J. Chen and L. Fang, *Int. J. Pharm.*, 2012, **424**, 58–66.
30 C. Nilsson, K. Edwards, J. Eriksson, S. W. Larsen, J. Østergaard, C. Larsen, A. Urtti and A. Yaghmur, *Langmuir*, 2012, **28**, 11755–11766.
31 B. J. Boyd, D. V. Whittaker, S. M. Khoo and G. Davey, *Int. J. Pharm.*, 2006, **318**, 154–162.
32 L. B. Lopes, D. A. Ferreira, D. De Paula, M. T. J. Garcia, J. A. Thomazini, M. C. A. Fantini and M. V. L. B. Bentley, *Pharm. Res.*, 2006, **23**, 1332–1342.
33 N. K. Swarnakar, V. Jain, V. Dubey, D. Mishra and N. K. Jain, *Pharm. Res.*, 2007, **24**, 2223–2230.
34 A. Angelova, B. Angelov, M. Drechsler, V. M. Garamus and S. Lesieur, *Int. J. Pharm.*, 2013, **454**, 625–632.
35 N. Bye, O. E. Hutt, T. M. Hinton, D. P. Acharya, L. J. Waddington, B. A. Mo, D. K. Wright, H. X. Wang, X. Mulet and B. W. Muir, *Langmuir*, 2014, **30**, 8898–8906.
36 B. W. Muir, D. P. Acharya, D. F. Kennedy, X. Mulet, R. A. Evans, S. M. Pereira, K. L. Wark, B. J. Boyd, T.-H. Nguyen, T. M. Hinton, L. J. Waddington, N. Kirby, D. K. Wright, H. X. Wang, G. F. Egan and B. A. Moffat, *Biomaterials*, 2012, **33**, 2723–2733.
37 C. Caltagirone, M. Arca, A. M. Falchi, V. Lippolis, V. Meli, M. Monduzzi, T. Nylander, A. Rosa, J. Schmidt, Y. Talmon and S. Murgia, *RSC Adv.*, 2015, **5**, 23443–23449.
38 Y. M. Yin, F. De Cui, C. F. Mu, M. K. Choi, J. S. Kim, S. J. Chung, C. K. Shim and D. D. Kim, *J. Controlled Release*, 2009, **140**, 86–94.
39 P. Zhao and D. Astruc, *ChemMedChem*, 2012, **7**, 952–972.
40 Y. Chen, L. Van Minh, J. Liu, B. Angelov, M. Drechsler, V. M. Garamus, R. Willumeit-Römer and A. Zou, *Colloids Surf., B*, 2016, **140**, 74–82.
41 Y. Chen, A. Angelova, B. Angelov, M. Drechsler, V. M. Garamus, R. Willumeit-Römer and A. Zou, *J. Mater. Chem. B*, 2015, **3**, 7734–7744.
42 B. Angelov, A. Angelova, S. K. Filippov, M. Drechsler, P. Štěpánek and S. Lesieur, *ACS Nano*, 2014, 5216–5226.

43 A. Angelova, B. Angelov, M. Drechsler and S. Lesieur, *Drug Discovery Today*, 2013, **18**, 1263–1271.
44 A. Angelova, B. Angelov, R. Mutafchieva and S. Lesieur, *J. Inorg. Organomet. Polym. Mater.*, 2015, 214–232.
45 C. Caltagirone, A. M. Falchi, S. Lampis, V. Lippolis, V. Meli, M. Monduzzi, L. Prodi, J. Schmidt, M. Sgarzi, Y. Talmon, R. Bizzarri and S. Murgia, *Langmuir*, 2014, **30**, 6228–6236.
46 V. Meli, C. Caltagirone, A. M. Falchi, S. T. Hyde, V. Lippolis, M. Monduzzi, M. Obiols-Rabasa, A. Rosa, J. Schmidt, Y. Talmon and S. Murgia, *Langmuir*, 2015, **31**, 9566–9575.
47 Y. Talmon, *J. Mol. Liq.*, 2015, **210**, 2–8.
48 L. Sagalowicz, M. Michel, M. Adrian, P. Frossard, M. Rouvet, H. J. Watzke, A. Yaghmur, L. De Campo, O. Glatter and M. E. Leser, *J. Microsc.*, 2006, **221**, 110–121.
49 M. Nakano, A. Sugita, H. Matsuoka and T. Handa, *Langmuir*, 2001, **17**, 3917–3922.
50 R. F. Kubin and A. N. Fletcher, *J. Lumin.*, 1982, **27**, 455–462.
51 M. Fischer and J. Georges, *Chem. Phys. Lett.*, 1996, **260**, 115–118.
52 A. Kazakevicĭus, D. Peckus, O. Boiko, L. Valkunas, E. Leonenko, G. Telbiz and V. Gulbinas, *J. Phys. Chem. C*, 2015, **119**, 19126–19133.
53 M. S. T. Gonçalves and M. S. T. Gonçalves, *Chem. Rev.*, 2009, **109**, 190–212.
54 D. Magde, G. E. Rojas and P. G. Seybold, *Photochem. Photobiol.*, 1999, **70**, 737–744.
55 V. Jain, N. K. Swarnakar, P. R. Mishra, A. Verma, A. Kaul, A. K. Mishra and N. K. Jain, *Biomaterials*, 2012, **33**, 7206–7220.
56 A. M. Falchi, A. Rosa, A. Atzeri, A. Incani, S. Lampis, V. Meli, C. Caltagirone and S. Murgia, *Toxicol. Res.*, 2015, **4**, 1025–1036.
57 A. Ganem-Quintanar, D. Quintanar-Guerrero and P. Buri, *Drug Dev. Ind. Pharm.*, 2000, **26**, 809–820.
58 M. Mosca, S. Murgia, A. Ceglie, M. Monduzzi and L. Ambrosone, *J. Phys. Chem. B*, 2006, **110**, 25994–26000.
59 L. B. Lopes, J. L. C. Lopes, D. C. R. Oliveira, J. A. Thomazini, M. T. J. Garcia, M. C. A. Fantini, J. H. Collett and M. V. L. B. Bentley, *Eur. J. Pharm. Biopharm.*, 2006, **63**, 146–155.
60 J. Barauskas, C. Cervin, M. Jankunec, M. Špandyreva, K. Ribokaitė, F. Tiberg and M. Johnsson, *Int. J. Pharm.*, 2010, **391**, 284–291.
61 T. M. Hinton, F. Grusche, D. Acharya, R. Shukla, V. Bansal, L. J. Waddington, P. Monaghan and B. W. Muir, *Toxicol. Res.*, 2014, **3**, 11–22.
62 N. Tran, X. Mulet, A. M. Hawley, T. M. Hinton, S. T. Mudie, B. W. Muir, E. C. Giakoumatos, L. J. Waddington, N. M. Kirby and C. J. Drummond, *RSC Adv.*, 2015, **5**, 26785–26795.
63 N. Tran, N. Bye, B. A. Moffat, D. K. Wright, A. Cuddihy, T. M. Hinton, A. M. Hawley, N. P. Reynolds, L. J. Waddington, X. Mulet, A. M. Turnley, M. C. Morganti-Kossmann and B. W. Muir, *Mater. Sci. Eng., C*, 2017, **71**, 584–593.